Contact mechanics of a gel under constrained swelling

Yue Zheng [a], Yuhang Hu [b], Shengqiang Cai [a,*]

[a] Department of Mechanical and Aerospace Engineering, University of California, San Diego, La Jolla, CA 92093, USA
[b] The George W. Woodruff School of Mechanical Engineering, Georgia Institute of Technology, Atlanta, GA 30332, USA

ARTICLE INFO

ABSTRACT

Gels have been widely explored in many engineering applications, in which they often swell with mechanical constraints. In this paper, we study mechanics of contact between a constrained swelling gel and a rigid spherical probe. We first derive an analytical form of the surface Green's function of a laterally constrained swelling gel occupying a half space. We then obtain an analytical form of the relationship between the indentation force and indentation depth for a spherical rigid indenter pressing onto a laterally constrained swelling gel, with and without taking account of the adhesion. Our theory also uncovers the influences of the constrained swelling ratio of the gel on the contact area (as well as its eccentricity), pull-off force and critical distance at separation. The essential parts of the analytical results are validated by finite element simulations. The results obtained in this article may help to better interpret experimental measurements from indentation tests of swollen gels.

© 2018 Elsevier Ltd. All rights reserved.

1. Introduction

Gels consist of crosslinked polymer networks and solvent molecules. Gels can swell or shrink by absorbing or extruding the solvent. The volume change of a gel can be as large as several hundred times of its original volume (Tanaka et al., 1982). By incorporating different functional groups on to the polymer chain, gels can be made stimuli responsive: swelling or shrinking in response to external stimuli, such as temperature (Hirotsu et al., 1987; Otake et al., 1990), pH (Tanaka et al., 1980), electric field (Tanaka et al., 1982), and light (Suzuki and Tanaka, 1990). The large deformation and stimuli-responsiveness of gels import them with many engineering applications, such as actuators (Bassil et al., 2008; Gerlach et al., 2005), sensors (Buenger et al., 2012; Richter et al., 2008), microfluidic device (Beebe et al., 2000; Dong et al., 2006), swellable packers (Cai et al., 2010), and many others.

Moreover, gels share many similarities to biological tissues, like low elastic modulus, high fluid content and high fluid permeability. Many synthetic gels are also biocompatible, making them ideal materials in biomedical applications such as drug delivery (Jeong et al., 1997; Merino et al., 2015; Qiu and Park, 2001), tissue engineering (Chaudhuri et al., 2015; Drury and Mooney, 2003; Lee and Mooney, 2001), and biosensors (Annabi et al., 2014; Peppas et al., 2006; Ulijn et al., 2007).

In both the engineering settings and the nature bio-systems, the gels and tissues are usually in confined spaces. For example, in the applications of self-regulating valves in microfluidic device (Beebe et al., 2000; Richter et al., 2004) and swellable packers in oil well (Kleverlaan et al., 2005; Qamar et al., 2012), the gels are bonded to rigid posts or pipes, and let swell against the outer boundary to completely seal the microfluidic channel or the oil well. Similarly in nature, plants use

---

* Corresponding author.
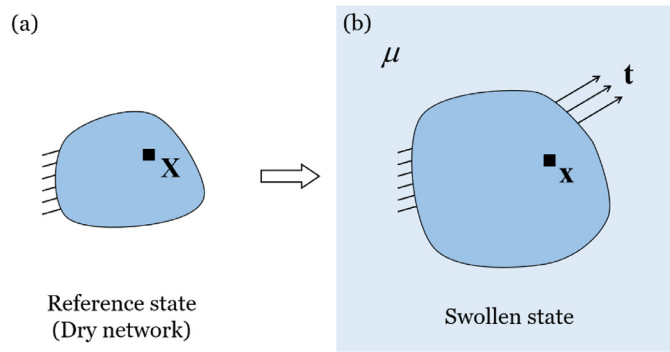 *E-mail address:* shqcai@ucsd.edu (S. Cai).

Fig. 1. Schematics of a gel in (a) reference state and (b) swollen state.

the constrained swelling gel to regulate the transport of water (Zwieniecki et al., 2001). Moreover, it is often the confined swelling of the brain in the rigid skull after traumatic brain injury (Goriely et al., 2016; Weickenmeier et al., 2016) that causes significant damages to the brain tissues. Therefore, understanding the contact mechanics of the gels under various constrained swelling conditions is of significant importance in generating new understandings of the biological tissues and guiding new engineering designs.

Another motivation of the current study lies in the recent ever-growing interests in using indentation to characterize the mechanical properties of gels and biological tissues due to its simple sample preparation and non-destructive feature (Constantinides et al., 2008; Ebenstein and Pruitt, 2004; Flanigan and Shull, 1999; Hu et al., 2012). Analytical study on the indentation of a constrained swelling gel could potentially improve the accuracy of the indentation tests of the soft gels and biological tissues (Miller et al., 2000; Rausch and Kuhl, 2013), and also promote new designs of indentation tests (Hui et al., 2006; Oyen, 2008).

In recent years, significant efforts have been made in studying the contact mechanics of gels. Based on linear poroelasticity, Hui and coworkers formulate a 2D Hertz problem of a horizontally placed rigid cylinder compressing a half-space gel (Hui et al., 2006). Closed-form solutions are derived for extracting the elastic properties and permeability of gels from indentation tests. The theory is also extended to cylindrical, conical, and spherical indenters, and the results are validated by FEM and experiments (Hu et al., 2010, 2011b; Lin and Hu, 2006). Later, a dynamic oscillation indentation method is also developed based on linear poroelasticity for characterizing gels in small scale using Atomic Force Microscope (Lai and Hu, 2017; Lin et al., 2007). To link the phenomenological poroelastic parameters to the thermodynamic properties of gels, the Flory–Huggins theory is employed and compared with the linear poroelasticity, demonstrating the significant effects of swelling on the properties of gels (Hu et al., 2011b). In addition to poroelastic indentation, works have also been done to study the viscoelastic and viscoporoelastic properties of gels using indentation (Galli et al., 2009; Kaufman et al., 2008; Liu et al., 2009; Strange et al., 2013). In all the previous work, the gel sample is assumed to be a half-space sample without any mechanical constraints and anisotropy. However, as mentioned previously, gels often undergo constrained swelling and it is known that the mechanical constraints opposed to the swelling gels have significant effects on the gel properties such as the effective stiffness and anisotropy (Chan et al., 2012; Delavoipière et al., 2016; Galli and Oyen, 2008; Hu et al., 2011a). So far, the effect of constrained swelling, especially the anisotropically constrained swelling, on the indentation of gels has not been systematically explored yet.

In the article, both the non-adhesive and adhesive contact mechanics between a rigid spherical probe and a constrained swelling gel are investigated. The paper is organized as follows. In Section 2, based on linear analysis, we obtain an analytical form of surface Green's function of a constrained swelling gel. In the first part of Section 2, the field theory of a constrained swelling gel is summarized; in the second part, by assuming that the additional deformation caused by a concentrated force on the surface of the gel is small, we formulate linearized governing equations and boundary conditions for the stress/strain field induced by the force. We solve the surface Green's function using Fourier transformation and the detailed process is listed in the Appendix. In Section 3, the indentation problem of the constrained swelling gel with a spherical indenter is solved, which is verified using finite element simulations. As in Section 4, the adhesion effect is taken into consideration based on JKR model. Concluding remarks of this study are included in Section 5.

2. Surface Green's function of a gel under constrained swelling

2.1. Nonlinear field theory of a constrained swelling gel

We first briefly summarize the nonlinear field theory of gels developed by Hong et al. (2008) and apply it to analyze the stress and strain field of a block of gel swelling in a solvent with mechanical constraints, as shown in Fig 1. In the current study, we assume the gel is always in an equilibrium state, indicating that the loading process on the gel is very slow. Taking the dry network as the reference state of the gel (Fig. 1(a)), a material element in the reference state is described by its

coordinate **X**. After the network absorbs the solvent and reaches an equilibrium state under mechanical load, the element **X** in the reference state moves to a new coordinate **x** in the swollen state (Fig. 1(b)). The deformation gradient is defined as $F_{iK} = \partial x_i / \partial X_K$.

In the swollen state, the chemical potential of the solvent in the gel reaches a constant value everywhere and equals the chemical potential of the solvent in the external solution μ. The nominal concentration of the solvent in the gel is donated as C, which is defined as the number of solvent molecules per unit volume of the dry polymer. As suggested in the previous work (Hong et al., 2008), the free energy density of the gel can be written as

$$\hat{W} = W_s + W_m - \mu C, \tag{1}$$

where W_s and W_m are the free energy contributions from stretching of polymer network and mixing between the polymer network and solvent, given by Flory–Rehner theory (Flory and Rehner Jr, 1943) as following:

$$W_s = \frac{1}{2} NkT [F_{iK} F_{iK} - 3 - 2 \log (\det \mathbf{F})], \tag{2}$$

$$W_m = -\frac{kT}{\Omega} \left[\Omega C \log \left(1 + \frac{1}{\Omega C} \right) + \frac{\chi}{1 + \Omega C} \right], \tag{3}$$

where N is the number of polymer chains per unit volume of dry polymers, T is the temperature, and k is the Boltzmann constant, Ω is the volume of a solvent molecule, and χ refers to a parameter measuring the enthalpy of mixing. Here we adopt the widely used assumption of molecular incompressibility, namely,

$$J = \det \mathbf{F} = 1 + \Omega C. \tag{4}$$

With the above assumption, the free energy of the gel becomes a function of deformation gradient **F** and chemical potential of solvent μ only, namely, $\hat{W} = \hat{W}(\mathbf{F}, \mu)$.

The nominal stress can be calculated from the free energy function as

$$s_{iK} = \frac{\partial \hat{W}}{\partial F_{iK}} (\mathbf{F}, \mu). \tag{5}$$

Combining Eqs. (1)–(5), we obtain that

$$s_{iK} = NkT [F_{iK} - (\zeta - \psi) H_{iK}], \tag{6}$$

with

$$\zeta = \frac{1}{N\Omega} \left(\frac{1}{J - 1} - \frac{2\chi}{J} \right) + 1, \tag{7}$$

$$\psi = \frac{J}{N\Omega} \left[\log \left(1 - \frac{1}{J} \right) + \frac{1}{J - 1} - \frac{\chi}{J^2} - \frac{\mu}{kT} \right], \tag{8}$$

where $H_{iK} \det \mathbf{F} = \partial (\det \mathbf{F}) / \partial F_{iK} = \frac{1}{2} e_{ijk} e_{KLM} F_{jL} F_{kM}$.

The nominal stress s_{iK} should satisfy the force balance equations:

$$s_{iK,K} = 0, \tag{9}$$

and boundary conditions:

$$s_{iK} N_K = T_i, \tag{10}$$

where **N** and **T** are the normal vector of the surface and nominal traction in the reference configuration.

We next consider a constrained swelling gel. The gel block is constrained in the x_1 and x_2 directions with prestretches: λ_1^{pre} and λ_2^{pre} in the two directions, respectively. The swelling ratio of the gel in the third direction λ_3 can be determined using the stress-free condition in the x_3 direction, namely,

$$s_{33} = 0. \tag{11}$$

Substituting $\mathbf{F}^0 = diag(\lambda_1^{pre}, \lambda_2^{pre}, \lambda_3)$ into Eqs. (6) and (11), we get

$$NkT \left(\lambda_3 - \frac{1}{\lambda_3} \right) + \frac{kT}{\Omega} \left[\lambda_1^{pre} \lambda_2^{pre} \log \left(1 - \frac{1}{\lambda_1^{pre} \lambda_2^{pre} \lambda_3} \right) + \frac{1}{\lambda_3} + \frac{\chi}{\lambda_1^{pre} \lambda_2^{pre} \lambda_3^2} - \lambda_1^{pre} \lambda_2^{pre} \frac{\mu}{kT} \right] = 0, \tag{12}$$

which can also be simply written as $\zeta - \psi = \lambda_3^2$ using the previously defined symbols in Eqs. (7) and (8).
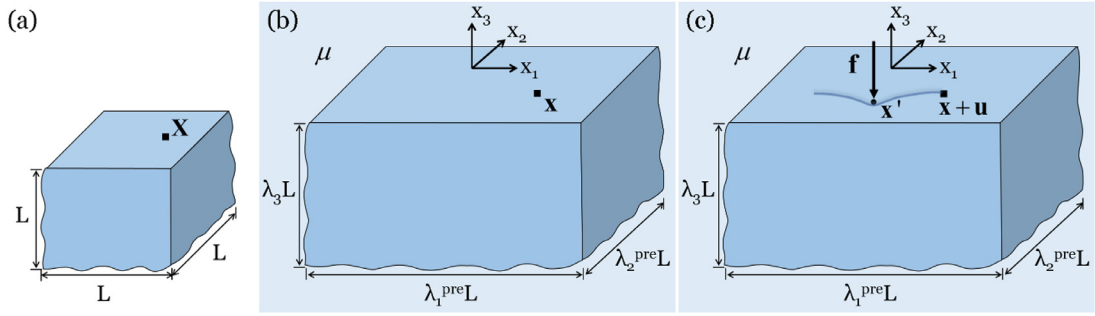
Fig. 2. (a) Each material element is marked by a coordinate **X** in the reference state (dry polymer). (b) In the constrained swelling state, the hydrogel swells and the chemical potential of the gel equilibrates with the chemical potential of the external solvent μ. The material element moves to the coordinate **x**. (c) A concentrated force **f**da is applied at **x**′ on the surface $x_3 = 0$, which perturbs the swollen gel with a field of infinitesimal deformation **u**.

2.2. Surface Green's function of a constrained swelling gel

Surface Green's functions for isotropic and anisotropic linear elastic solids have been obtained before (Barnett and Lothe, 1975; Lur'e, 1964; Willis, 1966), which have been successfully applied to solving several important linear elasticity problems (Eshelby, 1961; Gladwell, 1980; Mura, 2013; Vlassak et al., 2003; Willis, 1967). More recently, surface Green's function for a Neo-Hookean elastomer with arbitrarily large prestretch has also been obtained (He, 2008). Despite the wide applications of gels, the surface Green's function of a constrained swelling gel is not yet available. In this section, we will formulate the surface Green's function of a constrained swelling gel.

Following the nonlinear field theory of a gel summarized above, we regard a dry polymer network as the reference state, which occupies a half space as shown in Fig. 2(a). When the dry polymer network is prestretched and put in contact with a solvent, it can absorb solvent molecules, resulting in a constrained swelling gel as shown in Fig. 2(b). The prestretches of the gel in the two lateral directions are denoted by λ_1^{pre} and λ_2^{pre}. The swelling ratio of the gel in the vertical direction can be obtained by solving Eq. (12). To obtain the surface Green's function of a constrained swelling gel, as shown in Fig. 2(c), on the upper surface $x_3 = 0$, we apply a force **f**da on an infinitesimal element area da at the location: **x**′, which causes an incremental displacement field **u**. A material element with coordinate **x** in the constrained swelling state changes to $\bar{\textbf{x}}$ after a concentrated force is applied, which can be written as,

$$\bar{x}_i = x_i + u_i. \tag{13}$$

Therefore, the deformation gradient in the constrained swelling gel with an applied concentrated force is

$$\bar{F}_{iK} = F_{iK}^0 + \tilde{F}_{iK}, \tag{14}$$

where $F_{iK}^0 = \partial x_i / \partial X_K = \lambda_1^{pre}\delta_{i1}\delta_{K1} + \lambda_2^{pre}\delta_{i2}\delta_{K2} + \lambda_3\delta_{i3}\delta_{K3}$ and $\tilde{F}_{iK} = \partial u_i / \partial X_K = u_{i,k}F_{kK}^0$.

Similarly, the nominal stress in the gel with the applied concentrated force, which is denoted by $\bar{s}_{iK}$, can be written as:

$$\bar{s}_{iK} = s_{iK} + \tilde{s}_{iK}, \tag{15}$$

where $\bar{s}_{iK} = \partial \hat{W}(\bar{\textbf{F}}, \mu)/\partial F_{iK}$, and s_{iK} is the nominal stress in the constrained swelling gel without the application of the concentrated force: $s_{iK} = \partial \hat{W}(\textbf{F}^0, \mu)/\partial F_{iK}$.

If the additional deformation gradient, namely, $\tilde{F}_{iK}$ is small, we can keep just the linear order term of the difference between $\bar{s}_{iK}$ and s_{iK}, namely,

$$\tilde{s}_{iK} = \frac{\partial^2 \hat{W}(\textbf{F}^0, \mu)}{\partial F_{iK}\partial F_{kL}}\tilde{F}_{kL}. \tag{16}$$

Similar to Eqs. (9) and (10), the nominal stress $\bar{s}_{iK}$ should also satisfy the force balance equations and boundary conditions:

$$\bar{s}_{iK,K} = 0, \tag{17}$$

$$\bar{s}_{iK}N_K dA = f_i\delta(\textbf{x} - \textbf{x}')da \quad at \quad x_3 = 0, \tag{18}$$

where dA and da are the element area in the reference state and constrained swollen state respectively.

Subtracting Eqs. (9) and (10) from Eqs. (17) and (18), we have

$$\tilde{s}_{iK,K} = 0, \tag{19}$$

$$\tilde{s}_{iK}N_K dA = f_i\delta(\textbf{x} - \textbf{x}')da \quad at \quad x_3 = 0 \quad . \tag{20}$$

Using the formula of Nanson $JN_K dA = F^0_{jK} n_j da$, Eq. (20) can be rewritten as

$$\frac{\tilde{s}_{iK} F^0_{jK}}{J} n_j = f_i \delta(\mathbf{x} - \mathbf{x'}) \quad at \quad x_3 = 0 \quad . \tag{21}$$

The deformation in the swollen state is homogeneous, enabling the equivalent form of Eq. (19):

$$\left(\frac{\tilde{s}_{iK} F^0_{jK}}{J} \right)_{,j} = 0. \tag{22}$$

The term $\tilde{s}_{iK} F^0_{jK}/J$ in Eq. (21)–(22) can be expressed in terms of tensor using Eq. (16):

$$\frac{\tilde{s}_{iK} F^0_{jK}}{J} = C_{ijkl} u_{k,l}, \tag{23}$$

where C_{ijkl} can be regarded as incremental modulus tensor:

$$C_{ijkl} = \frac{NkT}{J} \left[\delta_{ik} F^0_{jK} F^0_{lK} + (\zeta - \psi) \delta_{il} \delta_{jk} + \psi \delta_{ij} \delta_{kl} \right]. \tag{24}$$

satisfying the symmetry $C_{ijkl} = C_{klij}$.

Eqs. (21) and (22) can be simplified as

$$C_{ijkl} u_{k,lj} = 0, \tag{25}$$

$$C_{ijkl} u_{k,l} n_j = f_i \delta(\mathbf{x} - \mathbf{x'}) \quad at \quad x_3 = 0. \tag{26}$$

Eqs. (25) and (26) are linearized governing equations for the incremental displacement field **u**. The general method of solving surface Green's function of an anisotropic linear elastic solid using Fourier transformation has been worked out by Willis (1966, 1967). The detailed process of solving Eqs. (25) and (26) and the complete form of the surface Green's function are given in Appendix. For brevity, here we only summarize the surface Green's function component $G_{33}(\mathbf{x} - \mathbf{x'})$, which is needed in the following sections.

$$G_{33}(\mathbf{x} - \mathbf{x'}) = \frac{1}{2\pi NkT} \frac{\lambda_1^{pre} \lambda_2^{pre} (t^2 - r^2) s}{\lambda_3 \left[(t^2 + r^2)^2 - 4r^2 ts \right]}, \tag{27}$$

in which r, t and s are

$$r = \sqrt{(x_1 - x_1')^2 + (x_2 - x_2')^2}, \tag{28}$$

$$t = \sqrt{\frac{\left(\lambda_1^{pre} \right)^2 (x_2 - x_2')^2 + \left(\lambda_2^{pre} \right)^2 (x_1 - x_1')^2}{\lambda_3^2}}, \tag{29}$$

$$s = \sqrt{\frac{\left(\lambda_1^{pre} \right)^2 (x_2 - x_2')^2 + \left(\lambda_2^{pre} \right)^2 (x_1 - x_1')^2 + r^2 \zeta}{\lambda_3^2 + \zeta}}. \tag{30}$$

3. Indentation of a constrained swelling gel by a rigid spherical indenter

3.1. Analytical results

With the surface Green's function obtained in Section 2, we are able to formulate the indentation problem of a constrained swelling gel. As an example, we consider a rigid spherical indenter of radius R pressing onto the surface of a constrained swelling gel, with prestretches λ_1^{pre} and λ_2^{pre} in two lateral directions. The schematic is shown in Fig. 3(a). The indentation depth is denoted by D. Due to the anisotropic swelling of the gel, the contact radii between the indenter and the gel in the x_1 and x_2 directions are generally different, which are denoted as a and b respectively. Both the lateral and vertical dimensions of the gel is assumed to be much larger than the radius of the indenter and the indentation depth, and thus the gel is assumed to occupy a half space in the following calculation. The contact between the indenter and the surface of the gel is assumed to be frictionless and non-adhesive in this section. We will consider the effect of adhesion in the next section as shown in Fig. 3(b).

It is noted that, in the current study, we assume the gel is always in an equilibrium state, indicating that the loading on the gel is slow enough. For the indentation of a gel, the characteristic length for the solvent diffusion in the gel is the indentation radius a, and the characteristic time for the solvent diffusion can be estimated as $t \sim a^2/D_s$, where D_s is the diffusivity of solvent in the gel. If we assume the indentation radius to be around 1 mm, we can estimate the characteristic
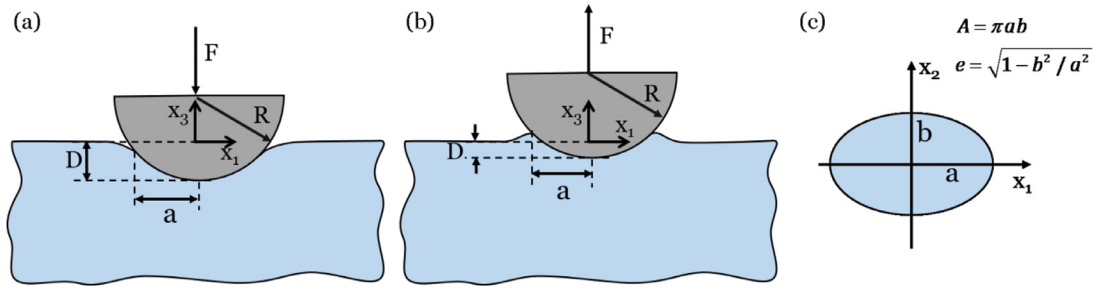
Fig. 3. Schematic of indentation on a constrained swelling gel (a) without adhesion and (b) with adhesion and (c) the corresponding contact area.

time for the gel to reach equilibrium to be around 100 s by using the diffusivity of water in gel $D_s = 10^{-8}$ m^2/s (Hu et al., 2010).

Willis (1966, 1967) has proved that for a linear elastic material, the contact area between the material and a rigid spherical indenter is an ellipse and the corresponding pressure distribution in the contact area takes the form:

$$p(\mathbf{x}) = p_0 \left(1 - \frac{x_1^2}{a^2} - \frac{x_2^2}{b^2} \right)^{1/2}, \tag{31}$$

where p_0 is the maximum pressure, a and b are the major and minor axes of the elliptical contact area as shown in Fig. 3(c), respectively. The values of these three parameters are to be determined by the relationship between the depth of indentation and the force applied onto the indenter.

The total force F applied on the indenter can be given by the integration:

$$F = \int\int_S p(\mathbf{x}) dx_1 dx_2 = \frac{2\pi}{3} p_0 ab. \tag{32}$$

Using surface Green's function, the normal displacement $u_3(\mathbf{x})$ caused by the pressure $p(\mathbf{x})$ can be calculated through the integration:

$$u_3(\mathbf{x}) = \int\int_S G_{33}(\mathbf{x} - \mathbf{x}') p(\mathbf{x}') dx_1' dx_2'. \tag{33}$$

We next perform the coordinate transformation:

$$x_1' = x_1 + r\cos\theta, \tag{34}$$

$$x_2' = x_2 + r\sin\theta. \tag{35}$$

Using Eqs. (34) and (35), we can rewrite the pressure distribution $p(\mathbf{x}')$ as

$$p(r, \theta) = \frac{p_0}{ab} \left[-(b^2\cos^2\theta + a^2\sin^2\theta)r^2 - 2r(b^2 x_1 \cos\theta + a^2 x_2 \sin\theta) + (a^2 b^2 - b^2 x_1^2 - a^2 x_2^2) \right]^{1/2}, \tag{36}$$

and the surface Green's function $G_{33}(\mathbf{x} - \mathbf{x}')$ as

$$G_{33}(r, \theta) = \frac{h(\theta)}{2\pi N k T r}, \tag{37}$$

with

$$h(\theta) = \frac{\lambda_1^{pre} \lambda_2^{pre} \left(g(\theta)^2 - 1 \right) f(\theta)}{\lambda_3 \left[\left(g(\theta)^2 + 1 \right)^2 - 4g(\theta) f(\theta) \right]}, \tag{38}$$

$$g(\theta) = \sqrt{\frac{\left(\lambda_1^{pre} \right)^2 \sin^2\theta + \left(\lambda_2^{pre} \right)^2 \cos^2\theta}{\lambda_3^2}}, \tag{39}$$

$$f(\theta) = \sqrt{\frac{\left(\lambda_1^{pre} \right)^2 \sin^2\theta + \left(\lambda_2^{pre} \right)^2 \cos^2\theta + \zeta}{\lambda_3^2 + \zeta}}. \tag{40}$$

In the polar coordinate system, Eq. (33) can be rewritten as:

$$u_3(\mathbf{x}) = \int_0^\pi \int_{r_1}^{r_2} G_{33}(r, \theta) p(r, \theta) r dr d\theta, \tag{41}$$

where the integration limits r_1 and r_2 are the two roots of the equation $(x_1 + r\cos\theta)^2/a^2 + (x_2 + r\sin\theta)^2/b^2 = 1$.

Eq. (41) can be integrated analytically and the result is:

$$u_3(\mathbf{x}) = \frac{bp_0}{4NkT}\left(I_0 - I_1\frac{x_1^2}{a^2} - I_2\frac{x_2^2}{a^2}\right), \tag{42}$$

with

$$I_0 = \int_0^\pi \frac{h(\theta)}{\left(1 - e^2\cos^2\theta\right)^{1/2}}d\theta, \tag{43}$$

$$I_1 = \int_0^\pi \frac{h(\theta)\sin^2\theta}{\left(1 - e^2\cos^2\theta\right)^{3/2}}d\theta, \tag{44}$$

$$I_2 = \int_0^\pi \frac{h(\theta)\cos^2\theta}{\left(1 - e^2\cos^2\theta\right)^{3/2}}d\theta, \tag{45}$$

where $e = \sqrt{1 - b^2/a^2}$ denotes the eccentricity of the contact area as shown in Fig. 3(c).

For a spherical indenter with radius R and indentation depth D, the displacement imposed by the surface profile of the rigid indenter can be approximated as,

$$u_3(\mathbf{x}) = D - \frac{1}{2R}x_1^2 - \frac{1}{2R}x_2^2. \tag{46}$$

Comparing Eq. (46) with (42), the calculated displacement agrees with the boundary condition when the following equations are satisfied

$$\frac{bp_0}{4NkT}I_0 = D, \tag{47}$$

$$\frac{bp_0}{4a^2NkT}I_1 = \frac{1}{2R}, \tag{48}$$

$$\frac{bp_0}{4a^2NkT}I_2 = \frac{1}{2R}. \tag{49}$$

Eqs. (48) and (49) indicate $I_1 = I_2$, which can be used to determine eccentricity e of the contact area:

$$\int_0^\pi \frac{h(\theta)\left(\cos^2\theta - \sin^2\theta\right)}{\left(1 - e^2\cos^2\theta\right)^{3/2}}d\theta = 0, \tag{50}$$

indicating that the eccentricity of the elliptical contact area is independent of indentation depth D.

We can also find that Eqs. (43)–(45) satisfy $I_0 = I_1 + (1 - e^2)I_2$. Combing this relationship with Eqs. (47)–(49), we can further obtain that

$$a = \sqrt{\frac{2RD}{2 - e^2}}. \tag{51}$$

The elliptical contact area is given by $A = \pi ab$, so that

$$A = 2\pi\frac{\sqrt{1 - e^2}}{2 - e^2}RD. \tag{52}$$

The maximum pressure p_0 is obtained by plugging Eq. (51) into Eq. (47),

$$p_0 = \frac{4NkT}{I_0}\sqrt{\frac{(2 - e^2)D}{2(1 - e^2)R}}. \tag{53}$$

Substituting Eq. (53) into Eq. (32), we have the force vs. depth relation of a constrained swelling gel indented by a rigid spherical indenter as:

$$F = \frac{8\pi NkT}{3I_0}\sqrt{\frac{2R}{2 - e^2}}D^{\frac{3}{2}}, \tag{54}$$

which shows that for a constrained swelling gel, the indentation force depends on the indentation depth to 3/2 power, similar to that for general linear elastic solids (Johnson, 1987). Due to the power law relation of Eq. (54), we can further normalize the indentation force by the indentation depth as:

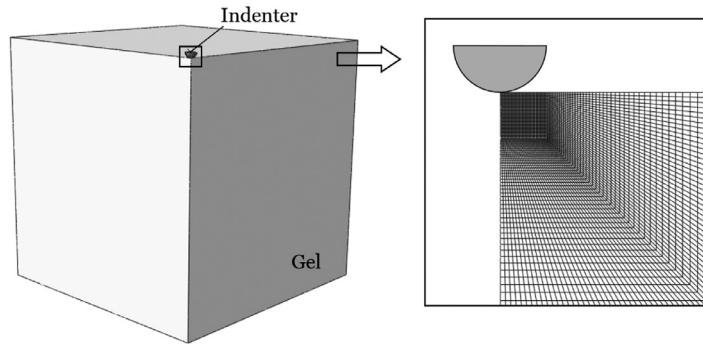$$\frac{F}{NkT\sqrt{RD^3}} = \frac{8\pi}{3I_0}\sqrt{\frac{2}{2 - e^2}}. \tag{55}$$

Fig. 4. Finite element simulation model of indentation on a constrained swelling gel.
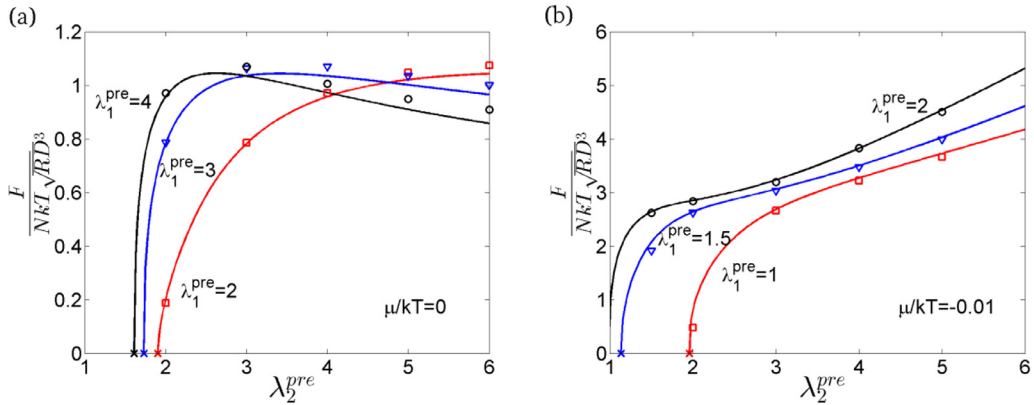

Fig. 5. Normalized indentation force as a function of constrained swelling ratios (λ_1^{pre} and λ_2^{pre}) with chemical potential (a) $\mu = 0$ and (b) $\mu/kT = -0.01$, where the solid lines are the theoretical predictions and the different symbols are the simulation results obtained from ABAQUS.

Consequently, the normalized indentation force in Eq. (55) only depends on the constrained swelling λ_1^{pre}, λ_2^{pre} and chemical potential μ, and is independent of indentation depth and radius of indenter.

The main analytical results obtained above are plotted together with finite element simulations as described in the following.

3.2. Comparison and discussion

To validate the above analytical results, we simulate the indentation of a constrained swelling gel using commercial finite element software ABAQUS with implemented user-defined subroutine (UHYPER) for gel materials (Hong et al., 2009). In the finite element model, a rigid spherical indenter is in contact with a block of swollen gel, and only a quarter of the gel is considered due to the symmetric geometry, as shown in Fig. 4. The width and height of the quarter gel block are set to be 50 times of the indenter radius with approximately 600,000 eight-node linear brick elements (C3D8). Mesh is further refined around the contact area and the element's lengths are around 1% of the indenter diameter (Fig. 4). Lateral displacement boundary conditions are applied at the side surfaces of the gel to maintain the prestretches, and then vertical displacement is applied on the indenter. The indentation force and deformation field of the gel are calculated by ABAQUS. The contact between the indenter and gel block is set to be frictionless and non-adhesive. For the parameters used in the simulation, $N\Omega = 0.001$ and $\chi = 0.1$.

According to Eq. (54), the indentation force depends on the indentation depth to 3/2 power, which is validated by the finite element simulation (the validation is not provided here). In the following plots, the force is further normalized as Eq. (55), which becomes independent of indentation depth. The normalized indentation force as a function of constrained lateral swelling ratios (λ_1^{pre} and λ_2^{pre}) with chemical potential $\mu = 0$ and $\mu/kT = -0.01$ is plotted in Fig. 5(a) and (b), where the solid lines are theoretical predictions and the different symbols are the simulation results obtained from ABAQUS. It is interesting to note that the relationship between the indentation force and lateral swelling ratio is not always monotonic. For instance, when $\lambda_1^{pre} = 3$ and $\lambda_1^{pre} = 4$ (Fig. 5(a)), the normalized indentation force increases and then decreases with the increase of λ_2^{pre}. Such nonmonotonic relationship results from the combination of the following two competing effects: it is found in our previous studies (Zheng et al., 2017) that for a Neo-Hookean solid, with the increase of lateral stretch, the indentation force increases; on the other hand, it is known, with the increase of the lateral stretch, the swelling ratio of
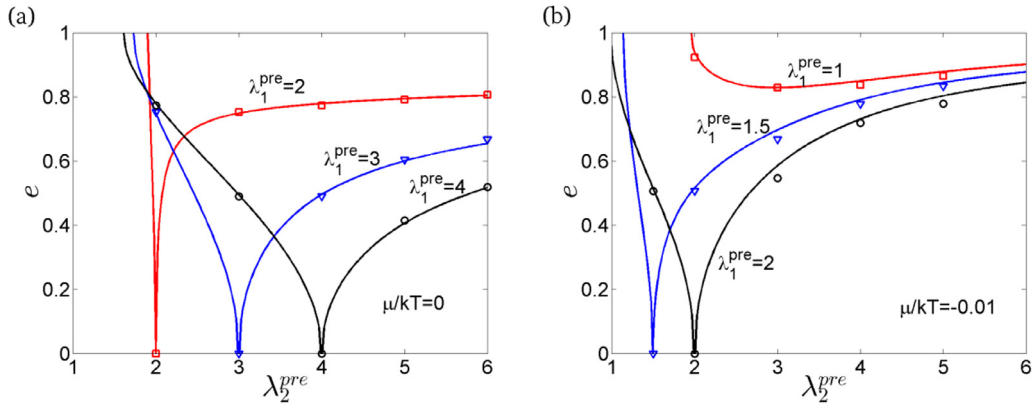
Fig. 6. The magnitude of the eccentricity of the contact area as a function of constrained swelling ratios (λ_1^{pre} and λ_2^{pre}) with chemical potential (a) $\mu = 0$ and (b) $\mu/kT = -0.01$, where the solid lines are the theoretical predictions and the different symbols are the simulation results obtained from ABAQUS.

Fig. 7. Normalized contact area as a function of constrained swelling ratios (λ_1^{pre} and λ_2^{pre}) with chemical potential (a) $\mu = 0$ and (b) $\mu/kT = -0.01$, where the solid lines are theoretical predictions and the different symbols are the simulation results obtained from ABAQUS.
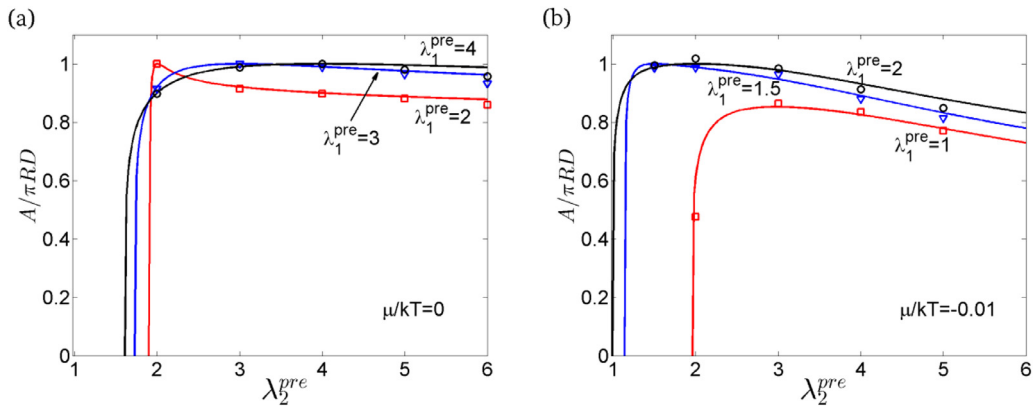
the gel increases, which dilutes the polymer content in unit volume of the gel and thus also reduces the stiffness of the gel (Hu et al., 2011b). This nonmonotonic relationship can only be observed when the chemical potential is close to zero, where the swelling ratio of the gel is very sensitive to the variation of its prestretch.

Another important prediction in Fig. 5(a) and (b) is that for certain combination of the constrained lateral swelling ratios, the normalized indentation force can drop to zero, which is clearly an indication of structural instability. Indeed, in previous studies (Kang and Huang, 2010; Weiss et al., 2013), it was found that for a laterally constrained swelling gel layer, surface wrinkle can appear when the constrained swelling ratios reach critical values. For three different λ_1^{pre} values, the critical prestretch ratio λ_2^{pre} values predicted in the previous studies are marked by cross in Fig. 5(a) and (b), which agree perfectly with the predictions from the current study.

In addition to the indentation force, we also plot the dependence of contact area on the constrained lateral swelling ratios for two different chemical potential values of the solvent. We plot the eccentricity of the contact area and the total contact area in Figs. 6 and 7 respectively, which can be used to fully determine the shape of the elliptical contact area. As shown in Fig. 6, the magnitude of the eccentricity reaches zero for equal-biaxial swelling, and increases with the increase of the difference between the swelling ratios in two lateral directions. There is one exception in Fig. 6(b) for $\lambda_1^{pre} = 1$: when λ_2^{pre} gets close to one, the magnitude of eccentricity increases rather than decreases. It can be understood as following: with the decrease of λ_2^{pre}, the swelling state of the gel approaches the critical condition (marked as crossing points at the horizontal axis in Fig. 5(a) and (b)) for surface wrinkling instability, resulting in great extension of the elliptical contact area in one direction.

Based on Eq. (52), we find that the normalized contact area $A/\pi DR$ decreases from 1 to 0 monotonically with the increase of the magnitude of eccentricity from 0 to 1. As a result, the contact area reaches maximum for equal-biaxial constrained swelling as shown in Fig. 7(a) and (b), expect for one case in Fig. 7(b) with $\lambda_1^{pre} = 1$ as explained above.

4. Adhesive contact between a rigid spherical indenter and a constrained swelling gel

In this section, we develop an analytical solution of a rigid spherical indenter pressing onto the surface of a constrained swelling gel with the consideration of the adhesion between the indenter and the gel (Fig. 3(b)), which is ignored in the above section. Following JKR theory (Johnson et al., 1971), we assume the pressure distribution in the elliptical contacting area has the following form:

$$p(\mathbf{x}) = p_0 \left(1 - \frac{x_1^2}{a^2} - \frac{x_2^2}{b^2}\right)^{1/2} + p_1 \left(1 - \frac{x_1^2}{a^2} - \frac{x_2^2}{b^2}\right)^{-1/2}, \tag{56}$$

where p_1 is negative.

Following the similar procedure as Section 3, the normal displacement caused by the pressure distribution in Eq. (56) can be integrated analytically as:

$$u_3(\mathbf{x}) = \frac{bp_0}{4NkT}\left(I_0 - I_1\frac{x_1^2}{a^2} - I_2\frac{x_2^2}{a^2}\right) + \frac{bp_1}{2NkT}I_0, \tag{57}$$

where I_0, I_1 and I_2 are the same as the ones given in Eqs. (43)–(45). The equation $I_1 = I_2 = I_0/(2 - e^2)$ is still satisfied, so that the eccentricity of the elliptical contact area is still determined by Eq. (50). In the current theory, the eccentricity of the contact area is not affected by adhesion, which has also been obtained in previous studies (Frétigny and Chateauminois, 2017; Gay, 2000).

In addition, we can also get the following equations by comparing Eq. (57) with Eq. (46):

$$p_0 = \frac{2NkT\left(2 - e^2\right)a^2}{I_0 R b}, \tag{58}$$

$$p_0 + 2p_1 = \frac{4NkTD}{I_0 b}. \tag{59}$$

The work done by the pressure will be stored as free energy in the gel system and also dissipated by solvent diffusion. In the current work, we assume the gel is always in an equilibriums state, or in another word, the load is very slowly applied, so the dissipated energy by solvent diffusion is negligible. It is also noted that the gel is initially equilibrated with the external solvent, and the gel is equilibrated with the external solvent again after loading, so the chemical potential of solvent does not change after loading. Consequently, the work done by the pressure is stored as elastic energy in the gel, namely:

$$U_E = \int\int_S \frac{1}{2} p(\mathbf{x})u(\mathbf{x})dx_1 dx_2. \tag{60}$$

Using Eqs. (58) and (59), Eq. (60) can be integrated as:

$$U_E = \frac{\pi NkT}{I_0}\left[2D^2 a - \frac{2\left(2 - e^2\right)D}{3R}a^3 + \frac{\left(2 - e^2\right)^2}{10R^2}a^5\right]. \tag{61}$$

According to JKR model, adhesion can decrease the surface energy by the amount of:

$$U_S = -\Delta\gamma\pi ab, \tag{62}$$

where $\Delta\gamma$ is the work of adhesion.

In the equilibrium state, it is assumed that the total energy reaches minimum, namely,

$$\frac{\partial U_E}{\partial a} + \frac{\partial U_S}{\partial a} = 0, \tag{63}$$

which results in

$$p_1 = -2\sqrt{\frac{NkT\Delta\gamma}{bI_0}}. \tag{64}$$

Combining Eqs. (58), (59), and (64), we have

$$D = \frac{\left(2 - e^2\right)a^2}{2R} - \sqrt{\frac{\Delta\gamma bI_0}{NkT}}. \tag{65}$$

The total force applied on the indenter can be calculated similarly as Eq. (32), that is

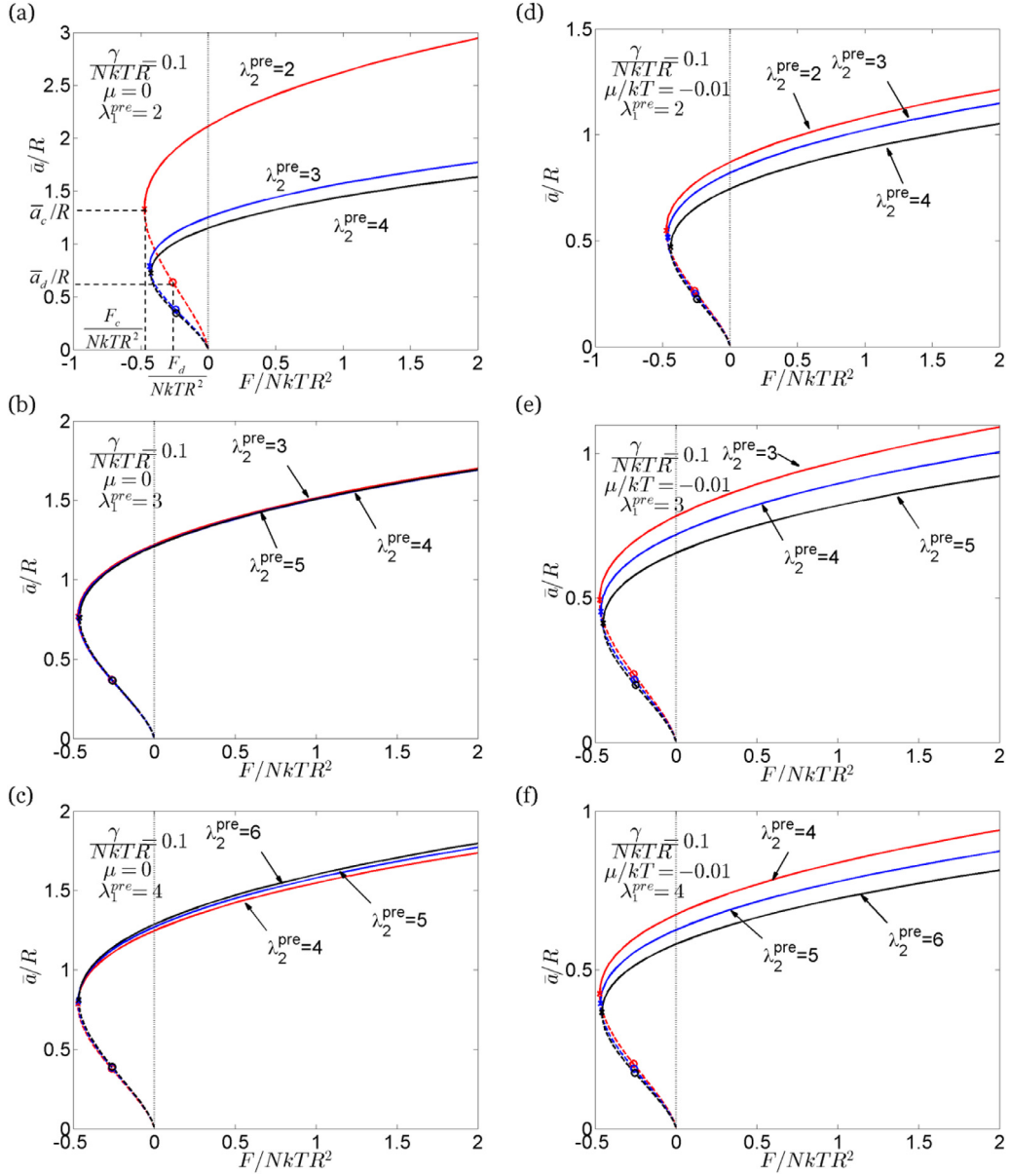$$F = \frac{2\pi}{3}p_0 ab + 2\pi p_1 ab. \tag{66}$$

Fig. 8. The relationship between mean contact radius and indentation force for a gel in different constrained swelling states with surface energy $\Delta\gamma/NkTR = 0.1$ and chemical potential (a)–(c) $\mu = 0$ and (d)–(f) $\mu/kT = -0.01$. The pull-off force F_c is marked with crosses and corresponding critical contact radius at separation is denoted as $\bar{a}_c$.

Substituting Eqs. (58) and (64) into Eq. (66), we obtain that

$$F = \frac{4\pi NkT\left(2 - e^2\right)a^3}{3Rl_0} - 4\pi\sqrt{\frac{NkT\Delta\gamma a^2 b}{l_0}}. \tag{67}$$

By introducing the definition of the mean contact radius as $\bar{a} = \sqrt{ab}$, we plot the radius $\bar{a}$ as a function of indentation force in Fig. 8(a)–(f), where the chemical potential of solvent is chosen to be $\mu = 0$ or $\mu/kT = -0.01$ and work of adhesion is fixed as $\Delta\gamma/NkTR = 0.1$.

The combination of Eqs. (65) and (67) fully determines the relationship between the indentation force and indentation depth. The result in Eq. (54) can be recovered by setting $\Delta\gamma = 0$ in Eqs. (65) and (67). The relationship between the indentation force and indentation depth for a gel in different constrained swelling states is plotted in Fig. 9(a)–(f), where the chemical potential of the solvent is chosen to be $\mu = 0$ or $\mu/kT = -0.01$ and the work of adhesion is fixed as $\Delta\gamma/NkTR = 0.1$.
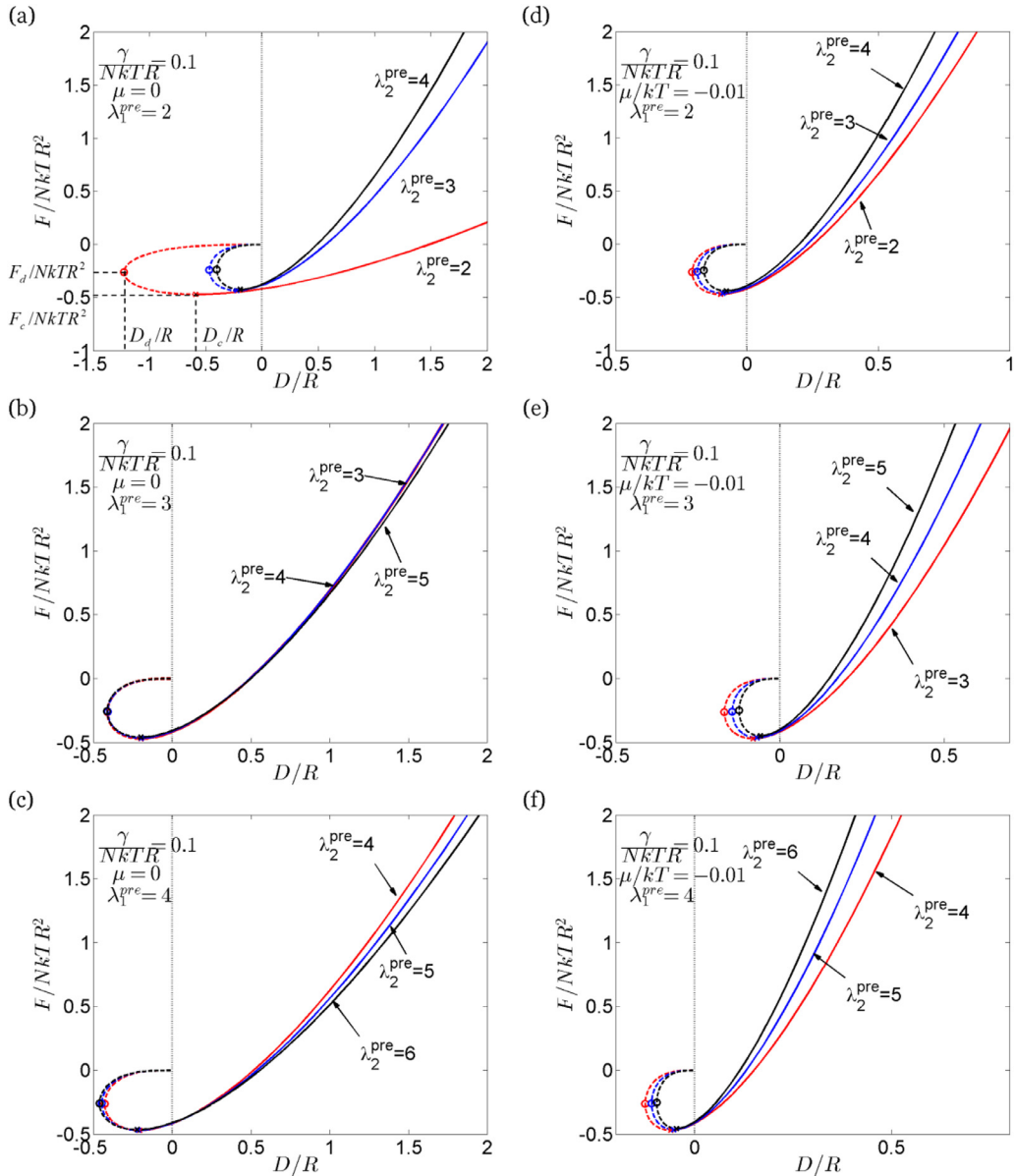
Fig. 9. The relationship between indentation force and indentation depth for a gel in different constrained swelling states with surface energy $\Delta\gamma/NkTR = 0.1$ and chemical potential (a)–(c) $\mu = 0$ and (d)–(f) $\mu/kT = -0.01$. The pull-off force F_c is marked by crosses and corresponding critical distance at separation is denoted by D_c.

When adhesion is considered, the relationship between the indentation force and indentation depth as shown in Fig. 9(a)–(f) no longer obeys the simple power law and becomes non-monotonic. More importantly, a tensile force can exist between the indenter and the gel surface, which corresponds to the negative force in Fig. 9(a)–(f). If the tensile force applied onto the indenter gradually increases from zero, the separation between the indenter and the gel surface happens when the tensile force reaches the maximal value (marked in Fig. 9(a)–(f)) which is denoted by F_c and often named as pull-off force. The corresponding distance between the indenter and the gel surface is denoted by D_c (also marked in Fig. 9(a)–(f)). Its value can be determined by using $dF/dD = 0$, together with Eq. (65) and Eq. (67), that gives $D_c = (\Delta\gamma/NkT)^{2/3}R^{1/3}[3I_0^2(1-e^2)/128(2-e^2)]^{1/3}$. Using the same three equations, we can also get the pull-off force $F_c = -3\pi R\Delta\gamma\sqrt{1-e^2}/(2-e^2)$, and the corresponding critical mean contact radius $\bar{a}_c = (\Delta\gamma/NkT)^{1/3}R^{2/3}[9I_0(1-e^2)^{5/4}/4(2-e^2)^2]^{1/3}$, which are marked in Fig. 8(a)–(f).

If the displacement of the indenter is controlled during pulling, the distance between the indenter and the gel surface can reach the maximal value before separation. The maximal distance is denoted by D_d and the corresponding force is
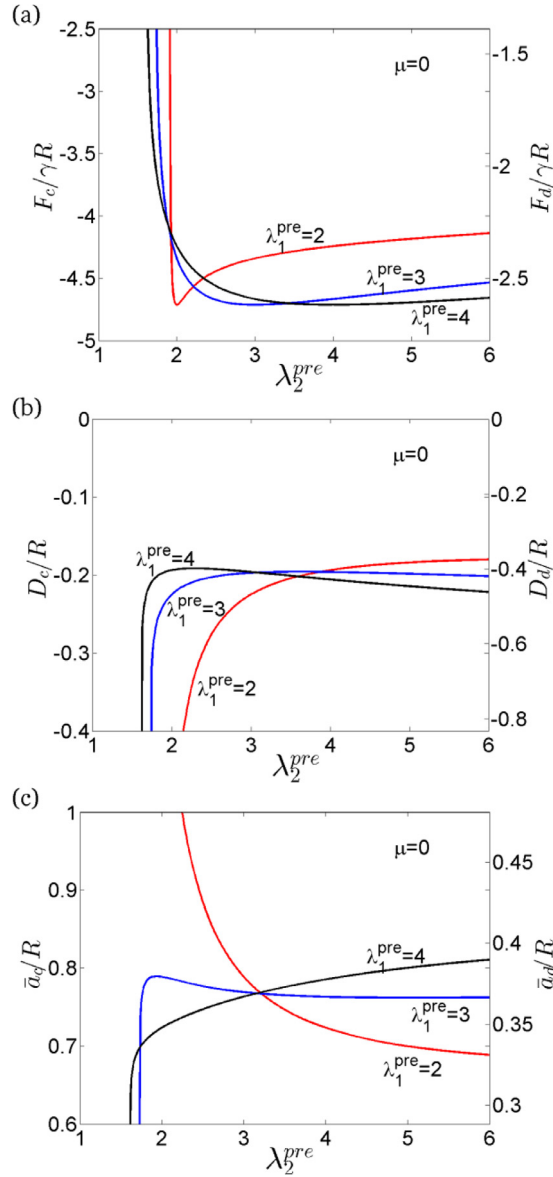
Fig. 10. (a) Pull-off force (F_c and F_d), (b) critical distance at separation (D_c and D_d) and (c) critical mean contact radius at separation ($\bar{a}_c$ and $\bar{a}_d$) as functions of constrained lateral swelling ratios with fixed chemical potential $\mu = 0$.

denoted by F_d, both of which are marked in Fig. 9(a)–(c). By solving Eqs. (65) and (67), together with $dD/dF = 0$, we can obtain that $D_d = 3^{2/3}D_c$. Using the same three equations, we can further get $F_d = 5/9F_c$ and the corresponding contact radius $\bar{a}_d = 3^{-2/3}\bar{a}_c$, which is also shown in Fig. 8(a)–(f).

In Fig. 10(a)–(c), we plot the pull-off force (F_c and F_d), critical distance at separation (D_c and D_d), and critical mean contact radius at separation ($\bar{a}_c$ and $\bar{a}_d$) as functions of one constrained lateral swelling ratio of the gel (λ_2^{pre}) with the other one fixed at three different values (λ_1^{pre}). We can clearly see from Fig. 10(a)–(c) that the constrained swelling state of a gel can have significant effects on the pull-off force, critical distance at separation, and critical contact radius at separation, which has not been discussed in previous studies.

At last, it is worth mentioning that for the adhesion theory adopted in the current work, the stress intensity factor is not a constant along the perimeter of the contact area. A new theory has been recently developed (Barber and Ciavarella, 2014; Johnson and Greenwood, 2005), in which the pressure distribution takes a different form and the stress intensity factors at the ends of the major and minor axes of the elliptical contact area can be enforced to be equal if the fracture toughness is isotropic. Consequently, the stress intensity factor from the new theory varies to a lesser extent along the perimeter of the contact area, with comparison to the current theory. In addition, the new theory predicts that the eccentricity of the

contact area can be load-dependent, in contrast to the prediction from the current work. However, we have confirmed that the relationship between the indentation force and indentation depth as well as the mean contact radius predicted by the new theory are very close to the ones predicted by the current work.

5. Conclusion

In this paper, we have studied both non-adhesive and adhesive contact mechanics between a laterally constrained swelling gel and a rigid spherical indenter. We have derived the surface Green's function of a laterally constrained swelling gel, which occupies a half space. Using the surface Green's function, we first formulate non-adhesive contact between a laterally constrained swelling gel and a rigid spherical indenter. Analytical relationship between the indentation force and indentation depth of a laterally constrained swelling gel is obtained. Due to the anisotropic prestretch in the two lateral directions, the contact area between the spherical indenter and the gel is generally elliptic. Our theory provides the analytical relationship between the contact area (as well as its eccentricity) and the prestretch ratios of the gel. Following the classical JKR model, we further expand the theory to take account of the effect of adhesion between the gel and the indenter. The theory developed in the article will potentially be helpful to extract more useful information from indentation tests of swelling gels and provide important insights in designing gel structures. It is worthwhile to mention that, based on the surface Green's function of a laterally constrained swelling gel derived in this article, many other important gel mechanics problems can be possibly formulated, such as adsorption of particles onto a gel surface and puncturing process of swelling gels.

Acknowledgment

Appendix

Eqs. (25)–(26) can be solved using Fourier transformation. Performing the Fourier transforms of displacement u_i in the x_1 and x_2 directions:

$$U_i(\boldsymbol{\xi}, x_3) = \int_{-\infty}^{+\infty} \int_{-\infty}^{+\infty} u_i(\mathbf{x}, x_3) e^{i\boldsymbol{\xi}\cdot\mathbf{x}} dx_1 dx_2, \tag{A1}$$

We can then express Eqs. (25)–(26) as

$$C_{i3k3} U_{k,33} - i\xi_\alpha (C_{i\alpha k3} + C_{i3k\alpha}) U_{k,3} - \xi_\alpha \xi_\beta C_{i\alpha k\beta} U_k = 0 \qquad \alpha, \beta = 1, 2, \tag{A2}$$

$$C_{ijkl} U_{k,l} n_j = f_i e^{i\boldsymbol{\xi}\cdot\mathbf{x}'} \quad at \quad x_3 = 0. \tag{A3}$$

According to Eq. (24), the nonzero components of modulus tensor are followings:

$$C_{1111} = \frac{NkT}{J}\left(\left(\lambda_1^{pre}\right)^2 + \zeta\right), \; C_{2222} = \frac{NkT}{J}\left(\left(\lambda_2^{pre}\right)^2 + \zeta\right), \; C_{3333} = \frac{NkT}{J}\left(\lambda_3^2 + \zeta\right), \tag{A4}$$

$$C_{2121} = C_{3131} = \frac{NkT}{J}\left(\lambda_1^{pre}\right)^2, \; C_{1212} = C_{3232} = \frac{NkT}{J}\left(\lambda_2^{pre}\right)^2, \; C_{1313} = C_{2323} = \frac{NkT}{J}\lambda_3^2, \tag{A5}$$

$$C_{1122} = C_{2211} = C_{1133} = C_{3311} = C_{2233} = C_{3322} = \frac{NkT}{J}\psi, \tag{A6}$$

$$C_{2112} = C_{1221} = C_{3113} = C_{1331} = C_{3223} = C_{2332} = \frac{NkT}{J}(\zeta - \psi). \tag{A7}$$

Substituting Eq. (A4)–(A7) into Eq. (A2) yields the transformed force balance equations

$$\lambda_3^2 U_{1,33} - i\zeta\xi_1 U_{3,3} - \left(\left(\lambda_1^{pre}\right)^2\xi_1^2 + \left(\lambda_2^{pre}\right)^2\xi_2^2 + \zeta\xi_1^2\right) U_1 - \zeta\xi_1\xi_2 U_2 = 0, \tag{A8}$$

$$\lambda_3^2 U_{2,33} - i\zeta\xi_2 U_{3,3} - \zeta\xi_1\xi_2 U_1 - \left(\left(\lambda_1^{pre}\right)^2\xi_1^2 + \left(\lambda_2^{pre}\right)^2\xi_2^2 + \zeta\xi_2^2\right) U_2 = 0, \tag{A9}$$

$$\left(\lambda_3^2 + \zeta\right) U_{3,33} - i\zeta\xi_1 U_{1,3} - i\zeta\xi_2 U_{2,3} - \left(\left(\lambda_1^{pre}\right)^2\xi_1^2 + \left(\lambda_2^{pre}\right)^2\xi_2^2\right) U_3 = 0. \tag{A10}$$

The ordinary differential equation system in Eq. (A8)–(A10) has the general solution $U_i(\boldsymbol{\xi}, x_3) = \sum_{A=1}^{6} c_i^A e^{m_A(\boldsymbol{\xi})x_3}$, and m_A can be solved from the characteristic equations:

$$m_{1,2} = \eta, m_3 = \gamma, m_{4,5} = -\eta, m_6 = -\gamma, \tag{A11}$$

where $\eta = \sqrt{(\lambda_1^{pre})^2 \xi_1^2 + (\lambda_2^{pre})^2 \xi_2^2}/\lambda_3$, $\gamma = \sqrt{(\lambda_1^{pre})^2 \xi_1^2 + (\lambda_2^{pre})^2 \xi_2^2 + (\xi_1^2 + \xi_2^2)\zeta}/\sqrt{\lambda_3^2 + \zeta}$. To meet the condition that the stress vanishes when x_3 approaches $-\infty$, only positive values in (A11) (m_1, m_2 and m_3) should be kept.

Substituting Eqs. (A4)–(A7) into Eq. (A3), and using the normal vector $n_j = \delta_{3j}$ at $x_3 = 0$, we can obtain the transformed boundary conditions

$$\lambda_3^2 U_{1,3} - i(\zeta - \psi)\xi_1 U_3 = \frac{J}{NkT} f_1 e^{i\boldsymbol{\xi}\cdot\mathbf{x}'}, \tag{A12}$$

$$\lambda_3^2 U_{2,3} - i(\zeta - \psi)\xi_2 U_3 = \frac{J}{NkT} f_2 e^{i\boldsymbol{\xi}\cdot\mathbf{x}'}, \tag{A13}$$

$$\left(\lambda_3^2 + \zeta\right) U_{3,3} - i\psi\xi_1 U_1 - i\psi\xi_2 U_2 = \frac{J}{NkT} f_3 e^{i\boldsymbol{\xi}\cdot\mathbf{x}'}. \tag{A14}$$

Plugging the general solution $U_i(\boldsymbol{\xi}, x_3) = c_i^1 e^{\eta x_3} + c_i^2 x_3 e^{\eta x_3} + c_i^3 e^{\gamma x_3}$ into Eqs. (A8)–(A10) and Eqs. (A12)–(A14), the parameters in the general solution can be determined

$$c_1^1 = \frac{1}{NkT}\frac{1}{\omega}\left[\frac{(\eta^2 + \xi^2)(\eta^2 + \xi_2^2) - 4\eta\gamma\xi_2^2}{\eta} f_1 + \frac{4\eta\gamma - (\eta^2 + \xi^2)}{\eta}\xi_1\xi_2 f_2 + 2\eta\gamma\xi_1 f_3 i\right] e^{i\boldsymbol{\xi}\cdot\mathbf{x}'}, \tag{A15}$$

$$c_2^1 = \frac{1}{NkT}\frac{1}{\omega}\left[\frac{4\eta\gamma - (\eta^2 + \xi^2)}{\eta}\xi_1\xi_2 f_1 + \frac{(\eta^2 + \xi^2)(\eta^2 + \xi_1^2) - 4\eta\gamma\xi_1^2}{\eta} f_2 + 2\eta\gamma\xi_2 f_3 i\right] e^{i\boldsymbol{\xi}\cdot\mathbf{x}'}, \tag{A16}$$

$$c_3^1 = \frac{1}{NkT}\frac{1}{\omega}\left[(\eta^2 + \xi^2)\xi_1 f_1 i + (\eta^2 + \xi^2)\xi_2 f_2 i - 2\xi^2\gamma f_3\right] e^{i\boldsymbol{\xi}\cdot\mathbf{x}'}, \tag{A17}$$

$$c_1^2 = c_2^2 = c_3^2 = 0, \tag{A18}$$

$$c_1^3 = \frac{1}{NkT}\frac{1}{\omega}\left[-2\eta\xi_1^2 f_1 - 2\eta\xi_1\xi_2 f_2 - (\eta^2 + \xi^2)\xi_1 f_3 i\right] e^{i\boldsymbol{\xi}\cdot\mathbf{x}'}, \tag{A19}$$

$$c_2^3 = \frac{1}{NkT}\frac{1}{\omega}\left[-2\eta\xi_1\xi_2 f_1 - 2\eta\xi_2^2 f_2 - (\eta^2 + \xi^2)\xi_2 f_3 i\right] e^{i\boldsymbol{\xi}\cdot\mathbf{x}'}, \tag{A20}$$

$$c_3^3 = \frac{1}{NkT}\frac{1}{\omega}\left[-2\eta\gamma\xi_1 f_1 i - 2\eta\gamma\xi_2 f_2 i + (\eta^2 + \xi^2)\gamma f_3\right] e^{i\boldsymbol{\xi}\cdot\mathbf{x}'}, \tag{A21}$$

where $\omega = \lambda_3[(\eta^2 + \xi^2)^2 - 4\xi^2\eta\gamma]/\lambda_1^{pre}\lambda_2^{pre}$ and ξ is the norm of $\boldsymbol{\xi}$. The above solutions work for the condition $\gamma \neq \eta$ and $\gamma \neq 0$.

Using the definition of surface Green's function $u_i(\mathbf{x}) = G_{ij}(\mathbf{x} - \mathbf{x}')f_j$, the transformed surface Green's function takes the form

$$\Gamma_{11}(\xi) = \frac{1}{NkT}\frac{(\eta^2 + \xi^2)(\eta^2 + \xi_2^2) - 4\eta\gamma\xi_2^2 - 2\eta^2\xi_1^2}{\omega\eta} e^{i\boldsymbol{\xi}\cdot\mathbf{x}'}, \tag{A22}$$

$$\Gamma_{22}(\xi) = \frac{1}{NkT}\frac{(\eta^2 + \xi^2)(\eta^2 + \xi_1^2) - 4\eta\gamma\xi_1^2 - 2\eta^2\xi_2^2}{\omega\eta} e^{i\boldsymbol{\xi}\cdot\mathbf{x}'}, \tag{A23}$$

$$\Gamma_{33}(\xi) = \frac{1}{NkT}\frac{(\eta^2 - \xi^2)\gamma}{\omega} e^{i\boldsymbol{\xi}\cdot\mathbf{x}'}, \tag{A24}$$

$$\Gamma_{12}(\xi) = \Gamma_{21}(\xi) = \frac{1}{NkT}\frac{(4\eta\gamma - \xi^2 - 3\eta^2)\xi_1\xi_2}{\omega\eta} e^{i\boldsymbol{\xi}\cdot\mathbf{x}'}, \tag{A25}$$

$$\Gamma_{13}(\xi) = -\Gamma_{31}(\xi) = \frac{1}{NkT} \frac{(2\eta\gamma - \eta^2 - \xi^2)\xi_1}{\omega} ie^{i\xi \cdot x'}, \tag{A26}$$

$$\Gamma_{23}(\xi) = -\Gamma_{32}(\xi) = \frac{1}{NkT} \frac{(2\eta\gamma - \eta^2 - \xi^2)\xi_2}{\omega} ie^{i\xi \cdot x'}. \tag{A27}$$

The surface Green's function can be further obtained using inverse Fourier transform

$$G_{11}(\mathbf{x} - \mathbf{x}') = \frac{1}{2\pi NkT} \frac{\lambda_1^{pre}\lambda_2^{pre}\left[(t^2 + r^2)\left(t^2 + (x_1 - x_1')^2\right) - 4ts(x_1 - x_1')^2 - 2t^2(x_2 - x_2')^2 \right]}{\lambda_3\left[(t^2 + r^2)^2 - 4r^2ts \right]t}, \tag{A28}$$

$$G_{22}(\mathbf{x} - \mathbf{x}') = \frac{1}{2\pi NkT} \frac{\lambda_1^{pre}\lambda_2^{pre}\left[(t^2 + r^2)\left(t^2 + (x_2 - x_2')^2\right) - 4st(x_2 - x_2')^2 - 2t^2(x_1 - x_1')^2 \right]}{\lambda_3\left[(t^2 + r^2)^2 - 4r^2ts \right]t}, \tag{A29}$$

$$G_{33}(\mathbf{x} - \mathbf{x}') = \frac{1}{2\pi NkT} \frac{\lambda_1^{pre}\lambda_2^{pre}(t^2 - r^2)s}{\lambda_3\left[(t^2 + r^2)^2 - 4r^2ts \right]}, \tag{A30}$$

$$G_{12}(\mathbf{x} - \mathbf{x}') = G_{21}(\mathbf{x} - \mathbf{x}') = \frac{1}{2\pi NkT} \frac{\lambda_1^{pre}\lambda_2^{pre}(4ts - r^2 - 3t^2)}{\lambda_3\left[(t^2 + r^2)^2 - 4r^2ts \right]t}(x_1 - x_1')(x_2 - x_2'), \tag{A31}$$

$$G_{13}(\mathbf{x} - \mathbf{x}') = -G_{31}(\mathbf{x} - \mathbf{x}') = \frac{1}{2\pi^2 NkT} \int_0^\pi \frac{\lambda_1^{pre}\lambda_2^{pre}(2pq - p^2 - r^2)\rho_1}{\lambda_3\left[(p^2 + r^2)^2 - 4r^2pq \right]\cos\theta} d\theta, \tag{A32}$$

$$G_{23}(\mathbf{x} - \mathbf{x}') = -G_{32}(\mathbf{x} - \mathbf{x}') = \frac{1}{2\pi^2 NkT} \int_0^\pi \frac{\lambda_1^{pre}\lambda_2^{pre}(2pq - p^2 - r^2)\rho_2}{\lambda_3\left[(p^2 + r^2)^2 - 4r^2pq \right]\cos\theta} d\theta. \tag{A33}$$

where

$$r = \sqrt{(x_1 - x_1')^2 + (x_2 - x_2')^2}, \tag{A34}$$

$$t = \sqrt{\frac{\left(\lambda_1^{pre}\right)^2(x_2 - x_2')^2 + \left(\lambda_2^{pre}\right)^2(x_1 - x_1')^2}{\lambda_3^2}}, \tag{A35}$$

$$s = \sqrt{\frac{\left(\lambda_1^{pre}\right)^2(x_2 - x_2')^2 + \left(\lambda_2^{pre}\right)^2(x_1 - x_1')^2 + r^2\zeta}{\lambda_3^2 + \zeta}}. \tag{A36}$$

$$\rho_1 = (x_1 - x_1')\cos\theta - (x_2 - x_2')\sin\theta, \tag{A37}$$

$$\rho_2 = (x_1 - x_1')\sin\theta + (x_2 - x_2')\cos\theta, \tag{A38}$$

$$p = \sqrt{\frac{\left(\lambda_1^{pre}\right)^2\rho_2{}^2 + \left(\lambda_2^{pre}\right)^2\rho_1{}^2}{\lambda_3^2}}, \tag{A39}$$

$$q = \sqrt{\frac{\left(\lambda_1^{pre}\right)^2\rho_2{}^2 + \left(\lambda_2^{pre}\right)^2\rho_1{}^2 + r^2\zeta}{\lambda_3^2 + \zeta}}. \tag{A40}$$

As stated before, the above solution only works for the condition $\gamma \neq \eta$ and $\gamma \neq 0$. When the conditions are not satisfied, degenerated solutions should be derived. There are only two cases when $\gamma = \eta$: one is that $\lambda_1^{pre} = \lambda_2^{pre} = \lambda_3$, which corresponds to the gel with isotropic swelling; the other is $\zeta = 0$, which is only possible when $\chi > 0.5$.

For the first case $\lambda_1^{pre} = \lambda_2^{pre} = \lambda_3 = \lambda$, the solution to Eq.(A2)–(A3) is

$$U_i(\boldsymbol{\xi}, x_3) = c_i^1 e^{\xi x_3} + c_i^2 x_3 e^{\xi x_3},$$ (A41)

in which

$$c_1^1 = \frac{1}{NkT} \frac{\lambda}{2\zeta} \left[\frac{(\lambda^2 + \zeta)\xi_1^2 + 2\zeta \xi_2^2}{\xi^3} f_1 + \frac{(\lambda^2 - \zeta)\xi_1 \xi_2}{\xi^3} f_2 + \frac{\lambda^2 \xi_1}{\xi^2} f_3 i \right] e^{i\boldsymbol{\xi} \cdot \mathbf{x}'},$$ (A42)

$$c_2^1 = \frac{1}{NkT} \frac{\lambda}{2\zeta} \left[\frac{(\lambda^2 - \zeta)\xi_1 \xi_2}{\xi^3} f_1 + \frac{(\lambda^2 + \zeta)\xi_2^2 + 2\zeta \xi_1^2}{\xi^3} f_2 + \frac{\lambda^2 \xi_2}{\xi^2} f_3 i \right] e^{i\boldsymbol{\xi} \cdot \mathbf{x}'},$$ (A43)

$$c_3^1 = \frac{1}{NkT} \frac{\lambda}{2\zeta} \left[-\frac{\lambda^2 \xi_1}{\xi^2} f_1 i - \frac{\lambda^2 \xi_2}{\xi^2} f_2 i + \frac{\lambda^2 + \zeta}{\xi} f_3 \right] e^{i\boldsymbol{\xi} \cdot \mathbf{x}'},$$ (A44)

$$c_1^2 = \frac{1}{NkT} \frac{\lambda}{2} \left[\frac{\xi_1^2}{\xi^2} f_1 + \frac{\xi_1 \xi_2}{\xi^2} f_2 + \frac{\xi_1}{\xi} f_3 i \right] e^{i\boldsymbol{\xi} \cdot \mathbf{x}'},$$ (A45)

$$c_2^2 = \frac{1}{NkT} \frac{\lambda}{2} \left[\frac{\xi_1 \xi_2}{\xi^2} f_1 + \frac{\xi_2^2}{\xi^2} f_2 + \frac{\xi_2}{\xi} f_3 i \right] e^{i\boldsymbol{\xi} \cdot \mathbf{x}'},$$ (A46)

$$c_3^2 = \frac{1}{NkT} \frac{\lambda}{2} \left[\frac{\xi_1}{\xi} f_1 i + \frac{\xi_2}{\xi} f_2 i - f_3 \right] e^{i\boldsymbol{\xi} \cdot \mathbf{x}'},$$ (A47)

The surface Green's function of the first case is

$$G_{11}(\mathbf{x} - \mathbf{x}') = \frac{1}{NkT} \frac{\lambda}{2\zeta} \frac{(\lambda^2 + \zeta)(x_2 - x_2')^2 + 2\zeta (x_1 - x_1')^2}{r^3},$$ (A48)

$$G_{22}(\mathbf{x} - \mathbf{x}') = \frac{1}{NkT} \frac{\lambda}{2\zeta} \frac{(\lambda^2 + \zeta)(x_1 - x_1')^2 + 2\zeta (x_2 - x_2')^2}{r^3},$$ (A49)

$$G_{33}(\mathbf{x} - \mathbf{x}') = \frac{1}{NkT} \frac{\lambda(\lambda^2 + \zeta)}{2\zeta} \frac{1}{r},$$ (A50)

$$G_{12}(\mathbf{x} - \mathbf{x}') = G_{21}(\mathbf{x} - \mathbf{x}') = \frac{1}{NkT} \frac{\lambda(\lambda^2 - \zeta)}{2\zeta} \frac{(x_1 - x_1')(x_2 - x_2')}{r^3},$$ (A51)

$$G_{13}(\mathbf{x} - \mathbf{x}') = -G_{31}(\mathbf{x} - \mathbf{x}') = \frac{1}{2\pi^2 NkT} \int_0^\pi \frac{\lambda^3}{2\zeta} \frac{\rho_1}{r^2 \cos\theta} d\theta,$$ (A52)

$$G_{23}(\mathbf{x} - \mathbf{x}') = -G_{32}(\mathbf{x} - \mathbf{x}') = \frac{1}{2\pi^2 NkT} \int_0^\pi \frac{\lambda^3}{2\zeta} \frac{\rho_2}{r^2 \cos\theta} d\theta.$$ (A53)

where r, ρ_1 and ρ_2 are defined as Eq. (A34) and (A37)-(A38).

For the second case $\zeta = 0$, the solution to Eq.(A2)–(A3) is

$$U_i(\boldsymbol{\xi}, x_3) = c_i e^{\eta x_3},$$ (A54)

with

$$c_1 = \frac{1}{NkT} \frac{\lambda_1^{pre} \lambda_2^{pre}}{(\eta^2 - \xi^2)\lambda_3} \left[\frac{\eta^2 - \xi_2^2}{\eta} f_1 + \frac{\xi_1 \xi_2}{\eta} f_2 + \xi_1 f_3 i \right] e^{i\boldsymbol{\xi} \cdot \mathbf{x}'},$$ (A55)

$$c_2 = \frac{1}{NkT} \frac{\lambda_1^{pre} \lambda_2^{pre}}{(\eta^2 - \xi^2)\lambda_3} \left[\frac{\xi_1 \xi_2}{\eta} f_1 + \frac{\eta^2 - \xi_1^2}{\eta} f_2 + \xi_2 f_3 i \right] e^{i\boldsymbol{\xi} \cdot \mathbf{x}'},$$ (A56)

$$c_3 = \frac{1}{NkT} \frac{\lambda_1^{pre} \lambda_2^{pre}}{(\eta^2 - \xi^2)\lambda_3} [-\xi_1 f_1 i - \xi_2 f_2 i + \eta f_3] e^{i\boldsymbol{\xi} \cdot \mathbf{x}'}.$$ (A57)

The surface Green's function of the second case is

$$G_{11}(\mathbf{x} - \mathbf{x}') = \frac{1}{NkT} \frac{\lambda_1^{pre}\lambda_2^{pre}}{\lambda_3} \frac{t^2 - (x_1 - x_1')^2}{(t^2 - r^2)t}, \tag{A58}$$

$$G_{22}(\mathbf{x} - \mathbf{x}') = \frac{1}{NkT} \frac{\lambda_1^{pre}\lambda_2^{pre}}{\lambda_3} \frac{t^2 - (x_2 - x_2')^2}{(t^2 - r^2)t}, \tag{A59}$$

$$G_{33}(\mathbf{x} - \mathbf{x}') = \frac{1}{NkT} \frac{\lambda_1^{pre}\lambda_2^{pre}}{\lambda_3} \frac{t}{(t^2 - r^2)}. \tag{A60}$$

$$G_{12}(\mathbf{x} - \mathbf{x}') = \frac{1}{NkT} \frac{\lambda_1^{pre}\lambda_2^{pre}}{\lambda_3} \frac{(x_1 - x_1')(x_2 - x_2')}{(t^2 - r^2)t}, \tag{A61}$$

$$G_{13}(\mathbf{x} - \mathbf{x}') = -G_{31}(\mathbf{x} - \mathbf{x}') = \frac{1}{2\pi^2 NkT} \int_0^\pi \frac{\lambda_1^{pre}\lambda_2^{pre}}{\lambda_3(p^2 - r^2)} \rho_1 d\theta, \tag{A62}$$

$$G_{23}(\mathbf{x} - \mathbf{x}') = -G_{32}(\mathbf{x} - \mathbf{x}') = \frac{1}{2\pi^2 NkT} \int_0^\pi \frac{\lambda_1^{pre}\lambda_2^{pre}}{\lambda_3(p^2 - r^2)} \rho_2 d\theta, \tag{A63}$$

where the definitions of r, t, ρ_1, ρ_2 and p are given in Eqs. (A34)–(A35) and (A37)–(A39).

Reference

Annabi, N., Tamayol, A., Uquillas, J.A., Akbari, M., Bertassoni, L.E., Cha, C., Camci-Unal, G., Dokmeci, M.R., Peppas, N.A., Khademhosseini, A., 2014. 25th anniversary article: rational design and applications of hydrogels in regenerative medicine. Adv. Mater. 26, 85–124.

Barber, J., Ciavarella, M., 2014. JKR solution for an anisotropic half space. J. Mech. Phys. Solids 64, 367–376.

Barnett, D., Lothe, J., 1975. Line force loadings on anisotropic half-spaces and wedges. Physica Norvegica 8, 13–22.

Bassil, M., Davenas, J., Tahchi, M.E., 2008. Electrochemical properties and actuation mechanisms of polyacrylamide hydrogel for artificial muscle application. Sens. Actuators, B 134, 496–501.

Beebe, D.J., Moore, J.S., Bauer, J.M., Yu, Q., Liu, R.H., Devadoss, C., Jo, B.-H., 2000. Functional hydrogel structures for autonomous flow control inside microfluidic channels. Nature 404, 588–590.

Buenger, D., Topuz, F., Groll, J., 2012. Hydrogels in sensing applications. Prog. Polym. Sci. 37, 1678–1719.

Cai, S., Lou, Y., Ganguly, P., Robisson, A., Suo, Z., 2010. Force generated by a swelling elastomer subject to constraint. J. Appl. Phys. 107, 103535.

Chan, E.P., Deeyaa, B., Johnson, P.M., Stafford, C.M., 2012. Poroelastic relaxation of polymer-loaded hydrogels. Soft Matter 8, 8234–8240.

Chaudhuri, O., Gu, L., Klumpers, D., Darnell, M., Bencherif, S.A., Weaver, J.C., Huebsch, N., Lee, H.-p., Lippens, E., Duda, G.N., 2015. Hydrogels with tunable stress relaxation regulate stem cell fate and activity. Nature Mater. 15 nmat4489.

Constantinides, G., Kalcioglu, Z.I., McFarland, M., Smith, J.F., Van Vliet, K.J., 2008. Probing mechanical properties of fully hydrated gels and biological tissues. J. Biomech. 41, 3285–3289.

Delavoipière, J., Tran, Y., Verneuil, E., Chateauminois, A., 2016. Poroelastic indentation of mechanically confined hydrogel layers. Soft Matter 12, 8049–8058.

Dong, L., Agarwal, A.K., Beebe, D.J., Jiang, H., 2006. Adaptive liquid microlenses activated by stimuli-responsive hydrogels. Nature 442, 551.

Drury, J.L., Mooney, D.J., 2003. Hydrogels for tissue engineering: scaffold design variables and applications. Biomaterials 24, 4337–4351.

Ebenstein, D., Pruitt, L., 2004. Nanoindentation of soft hydrated materials for application to vascular tissues. J. Biomed. Mater. Res. Part A 69, 222–232.

Eshelby, J., 1961. Elastic inclusions and inhomogeneities. Prog. Solid Mech. 2, 89–140.

Flanigan, C.M., Shull, K.R., 1999. Adhesive and elastic properties of thin gel layers. Langmuir 15, 4966–4974.

Flory, P.J., Rehner Jr, J., 1943. Statistical mechanics of cross-linked polymer networks I. Rubberlike elasticity. J. Chem. Phys. 11, 512–520.

Frétigny, C., Chateauminois, A., 2017. Contact of a spherical probe with a stretched rubber substrate. arXiv preprint arXiv:1703.06910.

Galli, M., Comley, K.S., Shean, T.A., Oyen, M.L., 2009. Viscoelastic and poroelastic mechanical characterization of hydrated gels. J. Mater. Res. 24, 973–979.

Galli, M., Oyen, M., 2008. Spherical indentation of a finite poroelastic coating. Appl. Phys. Lett. 93, 031911.

Gay, C., 2000. Does stretching affect adhesion? International journal of adhesion and adhesives 20, 387–393.

Gerlach, G., Guenther, M., Sorber, J., Suchaneck, G., Arndt, K.-F., Richter, A., 2005. Chemical and pH sensors based on the swelling behavior of hydrogels. Sens. Actuators, B 111, 555–561.

Gladwell, G.M., 1980. Contact Problems in the Classical Theory of Elasticity. Springer Science & Business Media.

Goriely, A., Weickenmeier, J., Kuhl, E., 2016. Stress singularities in swelling soft solids. Phys. Rev. Lett. 117, 138001.

He, L., 2008. Elastic interaction between force dipoles on a stretchable substrate. J. Mech. Phys. Solids 56, 2957–2971.

Hirotsu, S., Hirokawa, Y., Tanaka, T., 1987. Volume-phase transitions of ionized N-isopropylacrylamide gels. J. Chem. Phys. 87, 1392–1395.

Hong, W., Liu, Z., Suo, Z., 2009. Inhomogeneous swelling of a gel in equilibrium with a solvent and mechanical load. Int. J. Solids Struct. 46, 3282–3289.

Hong, W., Zhao, X., Zhou, J., Suo, Z., 2008. A theory of coupled diffusion and large deformation in polymeric gels. J. Mech. Phys. Solids 56, 1779–1793.

Hu, Y., Chan, E.P., Vlassak, J.J., Suo, Z., 2011a. Poroelastic relaxation indentation of thin layers of gels. AIP.

Hu, Y., Chen, X., Whitesides, G.M., Vlassak, J.J., Suo, Z., 2011b. Indentation of polydimethylsiloxane submerged in organic solvents. J. Mater. Res. 26, 785–795.

Hu, Y., You, J.-O., Auguste, D.T., Suo, Z., Vlassak, J.J., 2012. Indentation: a simple, nondestructive method for characterizing the mechanical and transport properties of pH-sensitive hydrogels. J. Mater. Res. 27, 152–160.

Hu, Y., Zhao, X., Vlassak, J.J., Suo, Z., 2010. Using indentation to characterize the poroelasticity of gels. Appl. Phys. Lett. 96, 121904.

Hui, C.Y., Lin, Y.Y., Chuang, F.C., Shull, K.R., Lin, W.C., 2006. A contact mechanics method for characterizing the elastic properties and permeability of gels. Journal of Polymer Science Part B: Polymer Physics 44, 359–370.

Jeong, B., Bae, Y.H., Lee, D.S., Kim, S.W., 1997. Biodegradable block copolymers as injectable drug-delivery systems. Nature 388, 860–862.

Johnson, K., Greenwood, J., 2005. An approximate JKR theory for elliptical contacts. J. Phys., D 38, 1042.

Johnson, K., Kendall, K., Roberts, A., 1971. Surface energy and the contact of elastic solids. In: Proceedings of the Royal Society of London A: Mathematical, Physical and Engineering Sciences. The Royal Society, pp. 301–313.

Johnson, K.L., 1987. Contact Mechanics. Cambridge University Press.

Kang, M.K., Huang, R., 2010. Swell-induced surface instability of confined hydrogel layers on substrates. J. Mech. Phys. Solids 58, 1582–1598.

Kaufman, J.D., Miller, G.J., Morgan, E.F., Klapperich, C.M., 2008. Time-dependent mechanical characterization of poly (2-hydroxyethyl methacrylate) hydrogels using nanoindentation and unconfined compression. J. Mater. Res. 23, 1472–1481.

Kleverlaan, M., van Noort, R.H., Jones, I., 2005. Deployment of swelling elastomer packers in Shell E&P, SPE/IADC Drilling Conference. Soc. Pet. Eng..

Lai, Y., Hu, Y., 2017. Unified solution for poroelastic oscillation indentation on gels for spherical, conical and cylindrical indenters. Soft Matter 13, 852–861.

Lee, K.Y., Mooney, D.J., 2001. Hydrogels for tissue engineering. Chem. Rev. 101, 1869–1880.

Lin, W.-C., Shull, K.R., Hui, C.-Y., Lin, Y.-Y., 2007. Contact measurement of internal fluid flow within poly (n-isopropylacrylamide) gels. J. Chem. Phys. 127, 094906.

Lin, Y.-Y., Hu, B.-W., 2006. Load relaxation of a flat rigid circular indenter on a gel half space. J. Non-Cryst. Solids 352, 4034–4040.

Liu, K., VanLandingham, M.R., Ovaert, T.C., 2009. Mechanical characterization of soft viscoelastic gels via indentation and optimization-based inverse finite element analysis. J. Mech. Behav. Biomed. Mater. 2, 355–363.

Lur'e, A.I., 1964. Three-Dimensional Problems of the Theory of Elasticity. Interscience Publishers.

Merino, S., Martín, C., Kostarelos, K., Prato, M., Vaźquez, E., 2015. Nanocomposite hydrogels: 3D polymer–nanoparticle synergies for on-demand drug delivery. ACS Nano 9, 4686–4697.

Miller, K., Chinzei, K., Orssengo, G., Bednarz, P., 2000. Mechanical properties of brain tissue in-vivo: experiment and computer simulation. J. Biomech. 33, 1369–1376.

Mura, T., 2013. Micromechanics of Defects in Solids. Springer Science & Business Media.

Otake, K., Inomata, H., Konno, M., Saito, S., 1990. Thermal analysis of the volume phase transition with n-isopropylacrylamide gels. Macromolecules 23, 283–289.

Oyen, M.L., 2008. Poroelastic nanoindentation responses of hydrated bone. J. Mater. Res. 23, 1307–1314.

Peppas, N.A., Hilt, J.Z., Khademhosseini, A., Langer, R., 2006. Hydrogels in biology and medicine: from molecular principles to bionanotechnology. Adv. Mater. 18, 1345–1360.

Qamar, S., Pervez, T., Akhtar, M., Al-Kharusi, M., 2012. Design and manufacture of swell packers: Influence of material behavior. Mater. Manuf. Processes 27, 721–726.

Qiu, Y., Park, K., 2001. Environment-sensitive hydrogels for drug delivery. Adv. Drug Delivery Rev. 53, 321–339.

Rausch, M.K., Kuhl, E., 2013. On the effect of prestrain and residual stress in thin biological membranes. J. Mech. Phys. Solids 61, 1955–1969.

Richter, A., Howitz, S., Kuckling, D., Arndt, K.-F., 2004. Influence of volume phase transition phenomena on the behavior of hydrogel-based valves. Sens. Actuators, B 99, 451–458.

Richter, A., Paschew, G., Klatt, S., Lienig, J., Arndt, K.-F., Adler, H.-J.P., 2008. Review on hydrogel-based pH sensors and microsensors. Sensors 8, 561–581.

Strange, D.G., Fletcher, T.L., Tonsomboon, K., Brawn, H., Zhao, X., Oyen, M.L., 2013. Separating poroviscoelastic deformation mechanisms in hydrogels. Appl. Phys. Lett. 102, 031913.

Suzuki, A., Tanaka, T., 1990. Phase transition in polymer gels induced by visible light. Nature 346, 345–347.

Tanaka, T., Fillmore, D., Sun, S.-T., Nishio, I., Swislow, G., Shah, A., 1980. Phase transitions in ionic gels. Phys. Rev. Lett. 45, 1636.

Tanaka, T., Nishio, I., Sun, S.-T., Ueno-Nishio, S., 1982. Collapse of gels in an electric field. Science 218, 467–469.

Ulijn, R.V., Bibi, N., Jayawarna, V., Thornton, P.D., Todd, S.J., Mart, R.J., Smith, A.M., Gough, J.E., 2007. Bioresponsive hydrogels. Mater. Today 10, 40–48.

Vlassak, J., Ciavarella, M., Barber, J., Wang, X., 2003. The indentation modulus of elastically anisotropic materials for indenters of arbitrary shape. J. Mech. Phys. Solids 51, 1701–1721.

Weickenmeier, J., Kuhl, E., Goriely, A., 2016. The mechanics of decompressive craniectomy: bulging in idealized geometries. J. Mech. Phys. Solids 96, 572–590.

Weiss, F., Cai, S., Hu, Y., Kang, Kyoo, M., Huang, R., Suo, Z., 2013. Creases and wrinkles on the surface of a swollen gel. J. Appl. Phys. 114, 073507.

Willis, J., 1966. Hertzian contact of anisotropic bodies. J. Mech. Phys. Solids 14, 163–176.

Willis, J., 1967. Boussinesq problems for an anisotropic half-space. J. Mech. Phys. Solids 15, 331–339.

Zheng, Y., Crosby, A.J., Cai, S., 2017. Indentation of a stretched elastomer. J. Mech. Phys. Solids 107, 145–159.

Zwieniecki, M.A., Melcher, P.J., Holbrook, N.M., 2001. Hydrogel control of xylem hydraulic resistance in plants. Science 291, 1059–1062.